Carbon supported Ru-Ni and Ru-W catalysts for the transformation of hydroxyacetone and saccharides into glycol-derived primary amines

Joseph Boulos, F. Goc, T. Vandenbrouck, N. Perret, Jeremy Dhainaut, Sebastien Royer, F. Rataboul

Carbon supported Ru-Ni and Ru-W catalysts for the transformation of hydroxyacetone and saccharides into glycol-derived primary amines

Joseph Boulos,[a] Firat Goc,[b] Tom Vandenbrouck,[b] Noémie Perret,[b] Jérémy Dhainaut,[a] Sébastien Royer[*a] and Franck Rataboul[*b]

[a] *Univ. Lille, CNRS, Centrale Lille, Univ. Artois, Unité de Catalyse et de Chimie du solide, UMR 8181, 59000 Lille, France*

[b] *Univ Lyon 1, CNRS, Institut de Recherches sur la Catalyse et l'Environnement de Lyon, UMR 5256, 2 avenue Albert Einstein, 69626 Villeurbanne, France*

* franck.rataboul@ircelyon.univ-lyon1.fr
* sebastien.royer@univ-lille.fr

Abstract

Nitrogen-containing molecules are widely used for the synthesis of pharmaceuticals, polymers, surfactants, agrochemicals, and dyes. In the general context of green chemistry, it is important to form such compounds from biosourced reactants. Short-chain primary amines are of interest for applications in the polymer industry, like 2-aminopropanol, 1-aminopropan-2-ol, and 1,2-diaminopropane. These amines can be formed through the so-called (reductive) amination of oxygenated substrates, preferably in aqueous phase. This is possible with heterogeneous catalysts, however, effective systems that allow reactions in water and under mild conditions are still lacking. Herein, we report the use of an efficient and robust catalyst Ru-Ni/AC (AC: activated carbon) for the reductive amination of hydroxyacetone into 2-aminopropanol. With a 4.5%Ru-4.5%Ni/AC catalyst up to 55% yield was obtained (aqueous NH_3, 65 °C, 60 bar H_2, 3-5 h). The catalyst has been reused during 3 cycles demonstrating a good stability. As a prospective study, extension to the reactivity of (poly)carbohydrates (glucose, fructose, cellulose, *ie* possible biosourced precursors of hydroxyacetone) has been realized. Despite a lesser efficiency, 2-aminopropanol (9% yield of amines) has been formed from fructose, the first example from a carbohydrate. This was possible using a 7.5%Ru-36%W_xC/AC catalyst, composition allowing a one-pot retro-aldol cleavage into hydroxyacetone and reductive amination (aqueous NH_3, 180 °C, 75 bar H_2, 3 h). The transformation of cellulose through sequential reactions with a combination of 30%W_2C/AC and 7.5%Ru-36%W_xC/AC system gave 2% of 2-aminopropanol, corresponding to the first example of the formation of this amine from cellulose furthermore with heterogeneous catalysts.

1. Introduction

In the general context of sustainable chemistry, biosourced amines are of fundamental interest as end-products or as intermediates especially for the polymer industry. Direct renewable resources of amines are very scarce and only concern amino acids and polymeric chitin.[1] Therefore, to date the formation of biosourced amines mainly relies on the amination of molecules easily obtained from renewable resources especially those presenting hydroxyl or carbonyl functions.

In the frame of our recent study[2] on the catalytic transformation of polysaccharides into biosourced ethylene and propylene glycol, $HO-CH_2-CH_2-OH$ and $CH_3-CH(OH)-CH_2-OH$, respectively, we were interested in forming amino-derivatives of these glycols. This was inspired by the recent study of Sels and coll. who reported the aminolysis of glucose and xylose by alkylamines into the corresponding secondary or tertiary alkylamino-derivatives of ethylene and propylene glycol.[3] Depending on the conditions and substrates, yields between 30-80% were obtained for derivatives like TMEDA in the presence of a Ru/C catalyst. These alkyl amines are considered as important products, however we believe that the primary amine equivalents are also of prime interest, as monomers for the synthesis of partly biosourced polyamides.[4] Therefore, we investigated the formation of primary amines derived from propylene glycol namely 2-aminopropanol $CH_3-CH(NH_2)-CH_2-OH$, 1-aminopropan-2-ol $CH_3-CH(OH)-CH_2-NH_2$ and 1,2-diaminopropane $CH_3-CH(NH_2)-CH_2-NH_2$.
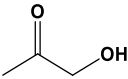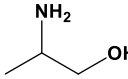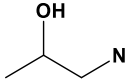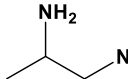
The direct amination of ethylene and propylene glycols or related molecules is not straightforward and, since the early report from Baiker *et al*. who reacted ethylene glycol with dimethylamine in the presence of Cu/Al_2O_3 catalyst,[5] only few studies have been reported (see Table S1 in Supplementary Information). Most of them involve NH_3 as aminating reagent to form primary amines, and the maximum reported yield of 2-aminopropanol is around 60% with a Co/La_3O_4 catalyst.[6]

Since the direct amination of alcohols is still a challenging catalytic reaction,[7] especially with biosourced substrates,[8] an alternative route is the catalytic reductive amination of a carbonyl function in the presence of hydrogen. This methodology has been well developed as shown by recent reviews.[9] Concerning heterogeneous catalysts, after the early studies on Ni-Raney®, systems based on precious metals were employed, particularly Ru. In general, the reductive amination is described for reactants having one oxygenated function, *i.e.* carbonyl.

Biosourced reactants may possess other reactive functions like hydroxyl, rending a selective transformation more difficult. Among them, furan derivatives have been by far the most studied because of the high reactivity of the carbonyl function leading to interesting products with preserved aromatic ring (5-hydroxymethyl-2-furfurylamine and 2,5-bis(aminomethyl)furan).[9a, d, g]

Based on this, we envisaged the formation of amines from glycols by the reductive amination of the biosourced intermediates/precursor of these glycols, *i.e.* glycoaldehyde $O=CH-CH_2-OH$ and hydroxyacetone $CH_3-C(=O)-CH_2-OH$, respectively. There are only a couple of examples describing the reductive amination of glycoaldehyde with catalysts, all based on supported Ru.[10] More reports exist concerning hydroxyacetone, but this remains limited (Table 1). They only concern the formation of primary amine derivatives (therefore with NH_3) using heterogeneous catalysis. This transformation is very challenging due to the need to combine conditions that are harsh enough to activate ammonia but mild enough to control the reaction.[11] Liang *et al.* reported the reductive amination with 5%Ru/ZrO$_2$ of a variety of aldehydes and ketones, with the example of hydroxyacetone producing 2-aminopropanol in 26% yield. The catalyst was formed of partly reduced Ru giving RuO_2 particles able to promote acid activation of the carbonyl group into imine intermediate, and Ru^0 particles for hydrogenation into amine. Trégner *et al.* proposed the use of 69%NiO/Al$_2$O$_3$ for a gas phase transformation giving at full conversion 45% yield of 2-aminopropanol.[12] More recently, Sheng *et al.* reported among a wide range of carbonyl compounds the formation of 2-aminopropanol (70%) from hydroxyacetone and aqueous NH_3 or ammonia acetate catalyzed by Co$_2$P nanorods under low H_2 pressure.[13] In a different kind of study, Shin *et al.* reported the formation of optically active (L)-2-aminopropanol by asymmetric reductive amination using (S)-α-methylbenzylamine in the presence of a 10%Pd/SBA-15, a 30%Pd/NaY catalyst giving higher conversion but lower enantiomeric excess.[14]

Table 1. Literature data on the reductive amination of hydroxyacetone with NH_3.

Conditions	Reactant conversion (%)	Main aminated products yield (%)			Ref.
	hydroxyacetone	2-aminopropanol	1-aminopropan-2-ol	1,2-diaminopropane	
5%Ru/ZrO$_2$ 25% aqu.NH$_3$ 30 bar H$_2$ 65 °C, 6 h	not given	26	not given	10	[10b]
69%NiO/Al$_2$O$_3$ 1 bar NH$_3$ 1 bar H$_2$ 130 °C, gas phase	100	45	3	traces	[12]
Co$_2$P nanorods 25% aqu.NH$_3$ 5 bar H$_2$ 100 °C, 10 h	96	70	not given	not given	[13]
10%Pd/SBA-15 (S)-α-methylbenzylamine 3.5 bar H$_2$	80	not given 80% ee[a]	not given	not given	[14]

[a] *ee*: enantiomeric excess

Globally 2-aminopropanol is always the main amino product due to the higher reactivity of the carbonyl function, 1-aminopropan-2-ol and 1,2-diaminopropane being rarely observed or even mentioned. However, in all cases a significant amount of propylene glycol is formed. Figure 1 summarises the different pathways that could lead to these products. Hydroxyacetone can be mono-aminated into 2-aminopropanol (route 1a) or 1-aminopropan-2-ol (route 1b), or directly di-aminated into 1,2-aminopropane (route 1c). The scarce literature (Table 1) indicates that route 1a is privileged whatever the conditions. 1,2-Diaminopropane can also be formed from routes 2a and 2b. Here the literature presents only studies concerning route 2b, with a paper describing the use of Ni-Raney® in the presence of K$_2$CO$_3$ under drastic conditions (170 °C, 15 h) giving 90% selectivity for 55% conversion.[15] Also, a patent from BASF claims the use of metal supported catalysts at 120 bar and 165 °C giving 93% selectivity for 85% conversion.[16] Besides, the reductive amination competes with the

simple reduction into propylene glycol (route 1d), but at this stage the transformation of the latter into aminated derivatives is far less likely under such conditions (see Table S1).
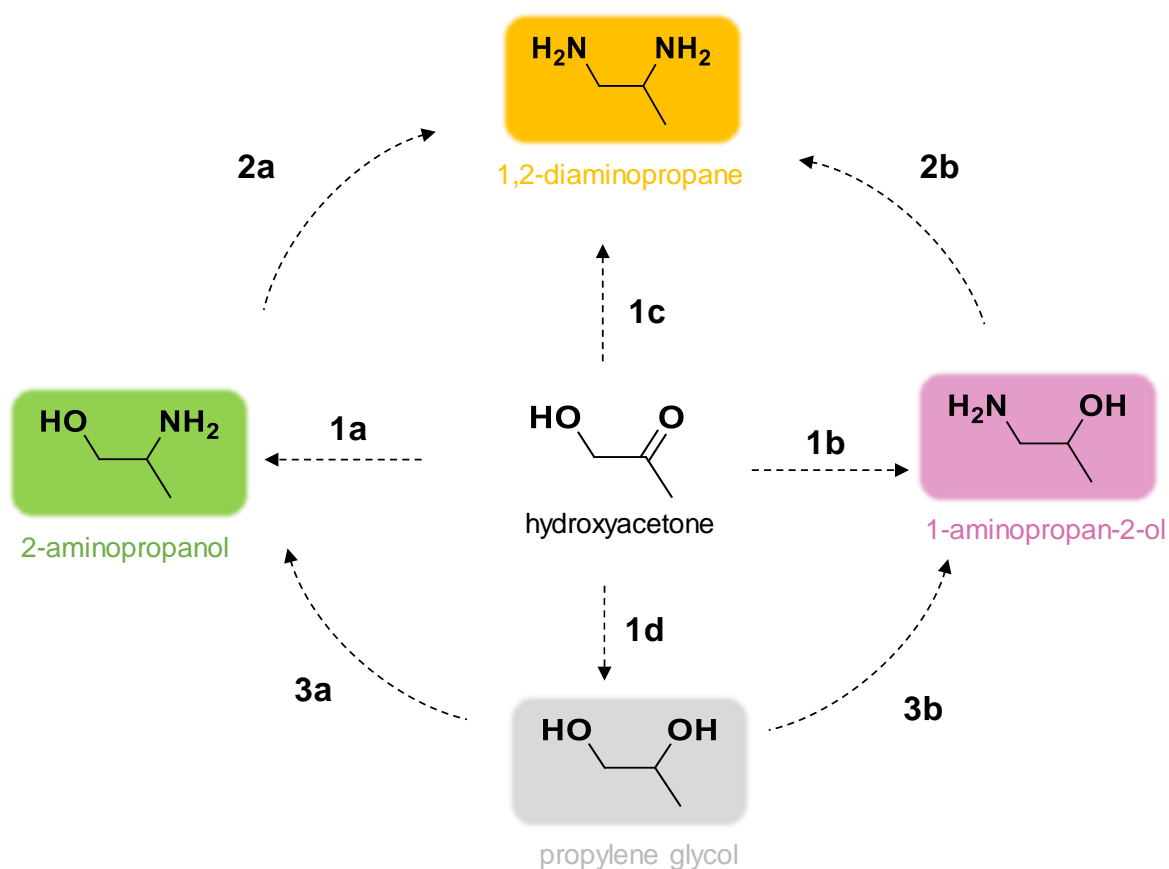
Figure 1. Possible reaction pathways involved in the reductive amination of hydroxyacetone by H_2/NH_3.

We present here a study on the formation of primary amino-derivatives of propylene glycol, by the reductive amination of hydroxyacetone by NH_3 in solution. For that, we investigated the properties of catalysts based on Ru active element. Effect of various reaction conditions and catalyst compositions will be presented, as well as the much more challenging sequential formation of aminated products from sugars and cellulose.

2. Experimental

2.1. Chemicals

L3S active carbon (AC) was obtained from Acticarbone/Chemviron; $Ni(NO_3)_2 \cdot 6H_2O$ ($\geq$ 97.0%) and $(NH_4)_{10}H_2(W_2O_7)_6$ ($\geq$ 99.0%) were purchased from Sigma and $Ru(NO)(NO_3)_3$ (Ru $\geq$ 31.3.%)

from Alfa Aesar; NH_3 aqueous solution (28-30 wt%) was obtained from Merck; hydroxyacetone ($\geq$ 90%), 2-aminopropanol ($\geq$ 98%), 1-aminopropan-2-ol ($\geq$ 93%), 1,2-diaminopropane ($\geq$ 99%), ethylene glycol ($\geq$ 99.8%), 1,2-propylene glycol, ($\geq$ 99.5%) glucose ($\geq$ 99.5%), fructose ($\geq$ 99 %) and Sigmacell cellulose (20 μm, DP ~ 250) were purchased from Sigma. All chemicals were used as received excepted cellulose that was dried before use (100 °C overnight).

2.2. Preparation of catalysts

2.2.1. x%Ru-y%Ni/AC

Under N_2 atmosphere, 2 g of AC were introduced in a 80 mL water solution of $Ru(NO)(NO)_3$ and $Ni(NO_3)_2 \cdot 6H_2O$ in a round-bottom flask. The mixture was stirred at room temperature for 4 h. After evaporation of water (60 °C, 200 mbar), the solid was dried at 80 °C overnight. The dry solid was introduced in a quartz reactor for reduction under H_2 flow (100 mL.min^{-1}, 2 °C.min^{-1}, 450 °C, 2 h). After cooling, the reactor was purged by Ar flow and the solid was passivated under O_2 (1 vol%) in N_2 flow for 6 h. Table 2 indicates the amount of precursors used to obtain the selected compositions, and the experimental compositions. Catalyst labelling refers to the label used in the main text.

2.2.2. 30%W₂C/AC and 5%Ni-30%W₂C/AC

These catalysts were prepared according to our previous study.[2]

2.2.3. 7.5%Ru-36%WₓC/AC

A 70 mL aqueous solution of 0.66 g $(NH_4)_{10}H_2(W_2O_7)_6$ was prepared under ultrasounds at 45 °C for 1 h. The solution was introduced in a round-bottom flask containing 0.25 g $Ru(NO_3)_3(NO)$ and 1 g of AC. The mixture was stirred at room temperature for 4 h. After water evaporation (60 °C, 200 mbar), the solid was dried at 80 °C overnight under N_2 atmosphere. The dry solid was introduced into a quartz reactor for temperature-programmed carburization under H_2 flow (100 mL.min^{-1}, 25-450 °C at 10 °C.min^{-1}, 450-700 °C at 1 °C.min^{-1}, 1 h). After cooling, the reactor was purged under Ar, and the solid was passivated under O_2 (1 vol%) in N_2 flow for 6 h.

6

Table 2. Composition of catalysts studied in this work.

Target comp. (wt%)	Mass[a] of Ru(NO)(NO$_3$)$_3$ (g)	Mass[a] of Ni(NO$_3$)$_2$·6H$_2$O (g)	Experim. comp.[b] (wt%)	Experim. comp.[b] (at%)	Catalyst labelling
5%Ni	-	0.52	Ni 5.6	Ni 1.2	5.5%Ni/AC
1%Ru	0.063	-	Ru 1.2	Ru 0.1	1%Ru/AC
5%Ru	0.33	-	Ru 5.3	Ru 0.7	5.3%Ru/AC
5%Ru-2.5%Ni	0.34	0.27	Ru 4.5; Ni 2.4	Ru 0.6; Ni 0.5	4.5%Ru-2.5%Ni/AC
5%Ru-5%Ni	0.35	0.55	Ru 4.6; Ni 4.4	Ru 0.6; Ni 1.0	4.5%Ru-4.5%Ni/AC
5%Ru-7.5%Ni	0.36	0.85	Ru 5.3; Ni 7.9	Ru 0.7; Ni 1.8	5.3%Ru-8%Ni/AC
1%Ru-5%Ni	0.067	0.53	Ru 1.2; Ni 5.1	Ru 0.2; Ni 1.1	1%Ru-5%Ni/AC

Target comp. (wt%)	Mass[a] of Ru(NO)(NO$_3$)$_3$ (g)	Mass[a] of (NH$_4$)$_{10}$H$_2$(W$_2$O$_7$)$_6$ (g)	Experim. comp.[b] (wt%)	Experim. comp.[b] (at%)	Catalyst labelling
5%Ru-30%W$_x$C	0.48	1.25	Ru 7.5; W 36	Ru 1.5; W 3.9	7.5%Ru-36%W$_x$C/AC

[a] for 2 g of AC [b] experimental composition determined by ICP-EOS, average of 2 sample analyses

2.3. Characterization

2.3.1. Elemental analyses

Metal loadings are expressed as relative mass contents (wt%) and were obtained by ICP-OES using a ACTIVA Horiba Jobin Yvon apparatus. The samples were mineralized with HNO$_3$-HF mixture, followed by final dissolution in concentrated H$_2$SO$_4$ at 100 °C overnight. Two analyses were conducted for each sample.

2.3.2. Textural analysis

The solids were initially heated under vacuum on a Micromeritics Smart VacPrep apparatus (250 °C, 1.10^{-6} bar, 2 h). Analyses were performed on a Micromeritics ASAP 2020 apparatus. The specific surface areas were calculated with the BET method from the obtained isotherms at p/p$_0$ between 0.05 to 0.25. The total pore volume was evaluated on the plateau of the

adsorption branch at p/p$_0$ = 0.98. The pore size was determined using the BJH method applied to the adsorption branch while the micropore volume was evaluated by the t-plot method.

2.3.4. X-Ray diffraction experiments

Diffractograms were obtained on a Bruker D8-Advance apparatus (LynxEye detector, Cu source, Ni filter in the 2θ = 10-80° range) and analyzed using DIFFRAC Eva software with JCPDS-ICDD-PDF4+ database for identification. Lattice parameters were obtained by performing Rietveld refinements using Topas 5.

2.3.5. X-ray photoelectron spectroscopy

Data were obtained on a KRATOS Axis Ultra spectrometer operating under ultrahigh vacuum conditions, employing a twin Al X-ray source (1486.6 eV) at a 40 eV pass energy. The pellet-shaped sample was fixed on a Cu holder. The binding energy values (B.E.) were estimated after positioning the C 1s peak of the contaminant carbon at 284.6 eV. The Casa XPS software was employed for data analysis.

2.3.6. CO chemisorption

CO chemisorption analysis was conducted on a Micromeritics 3-Flex instrument. The samples were reduced under H$_2$ (30 mL.min^{-1}) at 300 °C for 1 h, then flushed with Ar. CO uptake was measured at 0 °C. The particle sizes were estimated from irreversibly adsorbed CO with a CO-metal equal stoichiometry.

2.3.7. HRTEM analysis

Micrographs from High Resolution Transmission Electron Microscopy (HRTEM) were taken using TITAN Themis 300 S/TEM equipped with high brightness Schottkey field emission gun, a probe aberration corrector that allows energy and special resolution of about 150 meV and 70 pm respectively and a monochromator. The microscope is equipped with several annular dark field detectors as well as a super-X detector system with 4 windowless silicon drift detectors for the Electron Dispersive X-ray Spectroscopy (EDS). The experiments have been performed at 300 kV with semi-convergence angle of about 20 mrad, a probe size of the order of 500 pm and a probe current between 60 and 100 pA. For the high angle annular dark field (HAADF) imaging, c collection angles have been between 50 and 200 mrad. About 100 particles size were measured for each average particle size calculation. EDS mapping was obtained in spectrum imaging mode with a dwell time per pixel of about 15 µm and continuous scanning frames until total acquisition time of 15 to 20 minutes.

2.4. Reductive amination reactions

Experiments were performed in a 300 mL PARR Hastelloy reactor equipped with a mechanical stirrer. In a typical experiment, 10 g of hydroxyacetone and 1 g of catalyst were introduced in 100 mL of the NH_3 aqueous solution. The system was purged with argon then the reactor was stirred (1000 rpm), pressurized with H_2 and heated to the desired temperature. Note that the catalysts were passivated and then transferred directly to the reactor. After a certain time, the gas phase was evacuated, the liquid phase was collected and filtered under vacuum over Teflon 50 μm filter for analysis.

In case of gas phase collection, the reactor was cooled down to -80 °C using a liquid N_2/acetone bath, and H_2 was removed by pumping. After warm up to room temperature, the remaining gas phase was transferred into a gas collector cooled down to -80 °C. A mass of 150 mg was obtained analysed by MS and TCD.

A comment has been added in the Supplementary information concerning the choice and pertinency of the analytical method for the quantification of products. Quantification was performed using ^{13}C NMR on Brucker AVANCE spectrometer. Samples were prepared in DMSO-$d6$ in the presence of a known amount of dioxane as internal standard. The sequence has been optimized by adopting relaxation delay allowing the complete detection of each compound and the sample was analyzed over about 5000 scans. For NMR tube preparation, the order of magnitude corresponds to 0.5 g of reaction solution, 0.03 g of dioxane and 0.5 g of DMSO-d_6. ^{13}C NMR spectra of hydroxyacetone, and of the two main products 2-aminopropanol and propylene glycol, are presented in Figure S1. Signals used for quantification are that at 66.6 ppm for dioxane standard, 48.5 ppm for 1,2-diaminopropane CH_3-$CH(NH_2)$-CH_2-NH_2; 66.9 ppm for propylene glycol, 68.3 ppm for 1-aminopropan-2-ol CH_3-$CH(OH)$-CH_2-NH_2; 47.9 ppm for 2-aminopropanol CH_3-$CH(NH_2)$-CH_2-OH (Figure S2). The integration was set at 4 for the dioxane signal. ^{13}C NMR spectra of typical reaction mixtures are presented in Figures S3 and S4.

The amount of total organic carbon in the liquid phase was obtained on Shimadzu TOC-V_{CSH} apparatus. The carbon balance was determined by the ratio between the amount of organic carbon present in the liquid phase at the end of the reaction and the amount of organic carbon introduced.

For the recycling experiments, at the end of each run we tried to collect a maximum of the residual humid catalyst (with a small loss from the initial quantity), to be used it in the next run. For the hot filtration experiments, 100 mL of 25% aqueous NH_3, 10 g of hydroxyacetone

and 1 g of catalyst were introduced into the reactor. The catalyst was filtered from the reaction media after the first reaction (1 h at 65 °C and 60 bar H_2), 1 g of fresh hydroxyacetone was added to the filtrate and a second reaction was launched for 3 h at 65 °C and 60 bar H_2.

3. Results and discussion

3.1. Initial studies with 5.3Ru/AC catalyst

In the Introduction we saw that several catalysts based on metals like Ru, Ni, Pd, Co, supported on oxides or carbons, have been assessed for the production of amino-derivatives of ethylene and propylene glycol, starting from either the glycols themselves (Table S1), their carbonylated derivatives (Table 1), and even sugars.[3b]

We focused the first part of this study on a Ru/AC catalyst for the synthesis of 2-aminopropanol from hydroxyacetone, such system having never been used for this reaction. For that we initially prepared a catalyst with a 5.3%Ru/AC composition (see Section 3.2 for characterization details).

As a first set of experiments, the effects of reaction conditions were evaluated, time, temperature, and H_2 pressure. Figure 2 presents the results obtained with aqueous NH_3, employing reaction conditions inspired from the literature.[10b, 13]
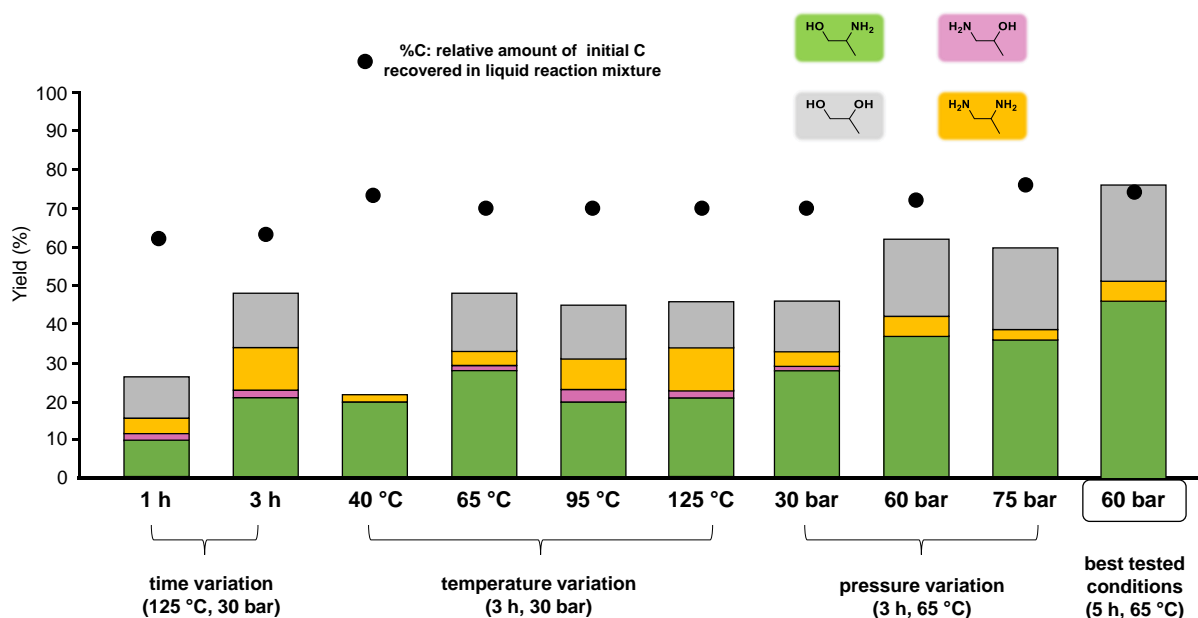

Figure 2. Condition variations for the reductive amination of hydroxyacetone in the presence of 5.3%Ru/AC. Conditions set: 100 mL of 25% aqueous NH_3, 10 g of hydroxyacetone, 1 g of catalyst. Acetol conversion was 100%.

We first evaluated the reaction time at 125 °C under 30 bar of H_2. After 3 h the overall amine yield reached 35%, much more than after 1 h of reaction (15%). The products repartition corresponds to literature data, *i.e.* the clearly predominant formation of 2-aminopropanol (22% yield) (Figure 1, route 1a) and a lower amount of the two other amines (routes 1b and 1c). The side reaction forming propylene glycol (route 1d) is significant (12%) confirming the difficulty to get a very selective transformation. However, by decreasing the temperature down to 65 °C, the yield into the amino-derivatives, and especially 2-aminopropanol was slightly higher (29% yield). Going further down to 40 °C, the reaction became restricted to the routes 1a and 2a (and/or 1c) with the main formation of 2-aminopropanol, but in a lower amount (20%). The H_2 pressure was then evaluated from 30 to 75 bar, and a pressure of 60 bar, despite forming more undesired propylene glycol, gave the best result in terms of amine formation (43%). With these conditions of temperature (65 °C) and pressure (60 bar) we reinvestigated the reaction time and a significant increase in amines was observed after 5 hours with yields up to 50% including 45% of 2-aminopropanol.

In summary, among those evaluated, a temperature of 65 °C, a pressure of 60 bar and a time of 5 hours gave the highest amino-derivatives yield. If we compare to the rare reports in the literature, these conditions are close to those of Liang *et al.* for hydroxyacetone amination with the Ru/ZrO_2 catalyst (30 bar, 65 °C, 6 h). Our results support their findings, for example the lesser influence of pressure on the various products formation over temperature, while a high temperature is not particularly suitable for the formation of the target amines.[10b]

In the experiments presented in Figure 2, hydroxyacetone was never detected in the post-reaction solution so the conversion of the reactant was complete. However, the amount of products quantified by NMR did not always match with the carbon present in the liquid phase (%C in Figure 2). A ^{13}C NMR spectrum of a reaction mixture obtained after 3 h at 65 °C under 75 bar is displayed in Figure S3. It clearly indicates the presence of signals other than those associated to the products. This is why we reported the relative amount of initial C recovered in the liquid reaction mixture (%C), a carbon balance determined by the ratio between the amount of organic carbon present in the liquid phase at the end of the reaction and the amount of organic carbon introduced. This data can indicate if all the products have been identified, in our case by ^{13C} NMR spectroscopy.

Therefore, we can say that these signals due to non-identified side-products explaining the gap between the %C in solution and the total yield of quantified products. For comparison, a spectrum displayed in Figure S4 corresponding to a reaction mixture obtained after 5 h at 65 °C under 60 bar for which the %C in solution matches with the total amount of quantified products (see Figure 2) does not present such signals. We believe that these signals are not due to ethylene glycol and/or its aminated derivatives. They are also not due to secondary amines formation especially dimerization into dimethylpiperazines sometimes observed as side-product.[17] However, the formation of secondary amine formation [(CH$_3$)(HOCH$_2$)CH]$_2$NH through Schiff-base formation/hydrogenation sequence cannot be excluded, which is coherent with a higher H$_2$ pressure.[18]

Also, the %C analysis indicates if all the carbon introduced (i.e. from acetol) is present in the reaction mixture as products. Here we obtained a 60-70% carbon balance, therefore about 30-40% of initial amount of C are not recovered in the liquid phase. We attempted to collect the gas phase to see if any gaseous products have been formed (see Experimental section for details). Analysis indicates the presence of only H$_2$ and H$_2$O in the gaseous sample. Therefore, no transformation into gaseous products happened, which is not surprising according to the low reaction temperature. The gap of mass balance may be due to organic molecules remaining adsorbed on the surface of the catalyst.

As a first conclusion, one can say that a 5.3%Ru/AC catalyst was able to transform hydroxyacetone into propylene glycol-derived amines in a 50% yield, including 45% of 2-aminopropanol and the selectivity can be adjusted by choosing the appropriate reaction conditions. Notably, we always focused on using relatively mild conditions, and working in the greenest possible media, for example in aqueous solvents and in the absence of any additive like base or acids. This is very important in the frame of sustainable transformations.

3.2. Variation of catalyst composition

3.2.1. Characterization of catalysts

After these first experiments with a 5.3%Ru/AC catalyst, we explored the potential of catalysts presenting different compositions, with emphasis on Ru associated to Ni which has also shown a potential in amination reactions,[18-19] to report here the first study of bimetallic Ru-Ni/AC catalysts for amination reactions. This would have also the advantage to replace part of Ru by a lesser critical metal. Different compositions of 1%Ru-5%Ni, 4.5%Ru-4.5%Ni, 4.5%Ru-2.5%Ni, and

5.3%Ru-8%Ni, were prepared by co-impregnation (see Experimental section for details) and characterized. For all compositions, XRD diffractograms (Figure 3) indicate the absence of signals due to metallic Ru (JCPDS 006-0663, main peak at 43.4°), which implies the presence of small metal nanoparticles (< 4 nm). The three main peaks associated with metallic Ni (2Θ = 44.3°, 51.6°, 76.2°) are detected for 5.3%Ru-8%Ni/AC due to high Ni loading. A main crystallite size of 23 nm can be estimated based on Scherrer equation. The peaks are consistent with a fcc Fm-3m structure with a lattice parameter a = 3.53 Å, which can be attributed to either pure Ni (a = 3.45-3.54 Å) or RuNi alloy (a = 3.54-3.62 Å). There is no formation of RuNi alloy with a hcp structure (P 63/mmc) like previously reported.[20] The main peak attributed to Ni or RuNi can also be perceived in 1%Ru-5%Ni/AC, but it overlaps with a peak from the carbon support, which prevents an accurate estimation of crystallite size.
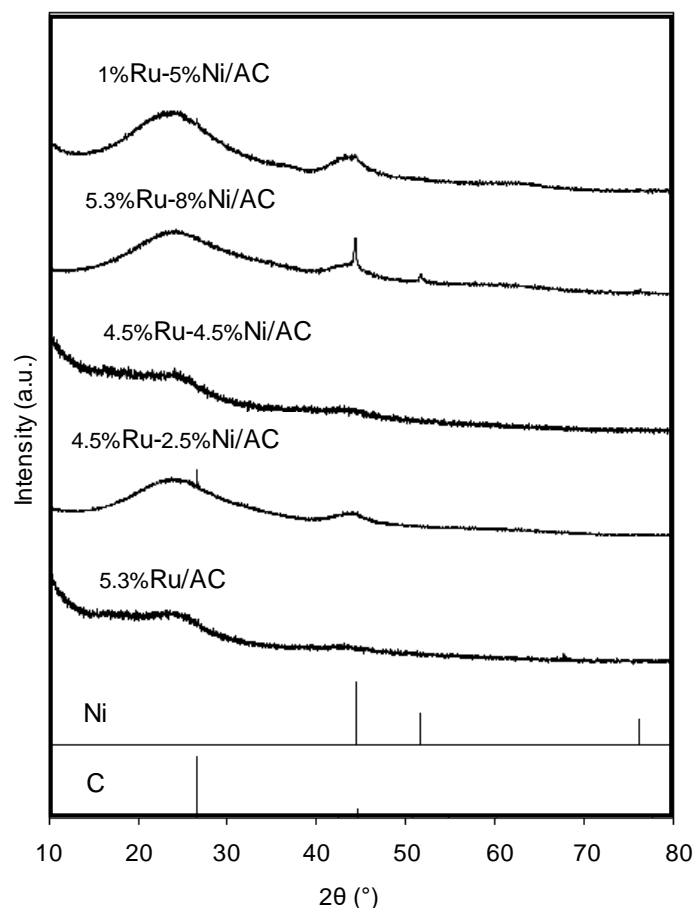

Figure 3. XRD diffractograms of AC-supported Ru and Ru-Ni catalysts. Peak assignments based on ICDD files C (PDF 00-025-0284) and Ni (PDF 04-002-7521).

Textural properties of these materials are presented in Table 3. The commercial AC presents a surface area of 905 $m^2.g^{-1}$, which has been retained for all Ru and Ru-Ni catalysts. Samples present type IV isotherms with H3-hysteresis loops at p/p_0 range 0.30-0.99, suggesting the

presence of both micropores and mesopores with a wedge-shaped pores arrangement (Figure S5).

Table 3. Textural properties of AC-supported Ru and Ru-Ni catalysts.

Catalyst	S_{BET}[a] $(m^2.g^{-1})$	S_μ[b] $(m^2.g^{-1})$	V_p[c] $(cm^3.g^{-1})$	V_μ[d] $(cm^3.g^{-1})$	d_{pore}[e] (nm)
5.3%Ru/AC	925	565	0.40	0.25	4-5
4.5%Ru-4.5%Ni/AC	940	540	0.40	0.25	4-5
1%Ru-5%Ni/AC	1060	620	0.45	0.25	4-5

[a] BET surface area [b] micropore surface area [c] total pore volume [d] micropore volume [e] BJH pore diameter calculated on the desorption branch

XPS measurements were performed on selected catalysts to identify the chemical states of the different elements. The Ru 3d, Ru 3p, Ni 2p, and C 1s core level XPS spectra of passivated 5.3%Ru/AC, 4.5%Ru-4.5%Ni/AC, and 1%Ru-5%Ni/AC are displayed in Figure 4. Table 4 reports the surface content of Ru and Ni and the oxidation state repartition of the different elements.

For all the samples, the C 1s spectra overlap with Ru 3d spectra (Figure 4a-c). Four main peaks are identified, located at 290.2 eV, 287.5 eV, 286.2 eV and 284.5 eV corresponding to C-C, C=O, C-O and C-C bonds, respectively.[21] For 5.3%Ru/AC, one oxidation state of Ru can be observed on Ru 3d spectrum, $Ru(OH)_2$, from the passivation layer ($3d_{5/2}$: 281 eV and 1 satellite: 283.7 eV; $3d_{3/2}$: 285.3 eV and 1 satellite: 287.9 eV) which was previously reported.[22] In order to further verify the oxidation state of Ru, we analyzed the Ru $3p_{3/2}$ spectrum (Figure 4d). The peaks at 462.5 eV and 465.5 eV (satellite peak) are also correlated to $Ru(OH)_2$.[22b, 23] 5.3%Ru/AC presents 14 at% of Ru concentration on the surface (Table 4) which is higher than the bulk composition determined by ICP-OES (0.7 at% of Ru in 5.3%Ru/AC, see Experimental section).

For 4.5%Ru-4.5%Ni/AC (Figure 5a) and 1%Ru-5%Ni/AC (Figure 5b), only Ru^{2+} associated with the passivation layer is observed, as previously. However, the main peaks were shifted by 0.4 eV due to Ru-Ni interactions[20] ($3d_{5/2}$: 280.6 eV and 1 satellite: 282 eV; $3d_{3/2}$: 284.8 eV and 1 satellite: 286.2 eV).[22a] Two oxidation states of Ni are also observed for all samples (Figure 5), (1) Ni^0 ($2p_{3/2}$: 852.6 eV and 2 plasmon loss peaks: 856.3 eV and 858.7 eV), (2) oxidized species $Ni(OH)_2$, due to the passivation step ($2p_{3/2}$: 854.9 eV and 5 satellites: 855.7 eV, 857.7 eV, 860.5 eV, 861.5 eV, and 866.5 eV).[24] 4.5%Ru-4.5%Ni/AC and 1%Ru-5%Ni/AC exhibit 6 and 5% atoms

14

of Ni^0 at the surface, which could be attributed to the hydrogen spillover capability of Ru to Ni.[25] 4.5%Ru-4.5%Ni/AC presents 14 at% of Ru and 7 at% of Ni concentrations on the surface (Table 4), which is higher than the bulk composition determined by ICP-OES (0.6 at% of Ru and 1 at% of Ni, Table 1). 1%Ru-5%Ni/AC presents 9 at% of Ru and 10 at% of Ni concentrations on the surface (Table 4), which is higher than the bulk composition determined by ICP-OES (0.2 at% of Ru and 1.1 at% of Ni, see Experimental section).
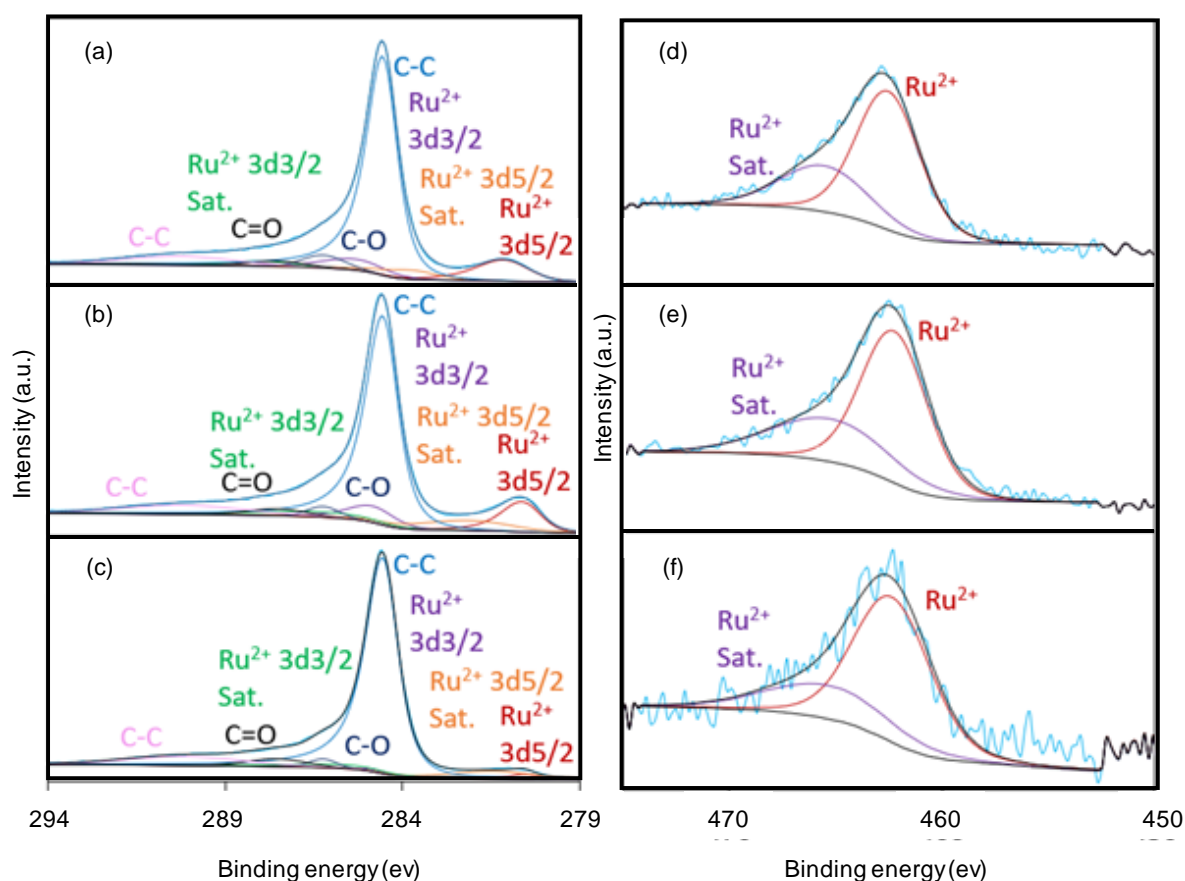

Figure 4. C 1s and Ru3d XPS spectra of (a) 5.3%Ru/AC, (b) 4.5%Ru-4.5%Ni/AC, (c) 1%Ru-5%Ni/AC; Ru 3p spectra of (d) 5.3%Ru/AC, (e) 4.5%Ru-4.5%Ni/AC, (f) 1%Ru-5%Ni/AC.
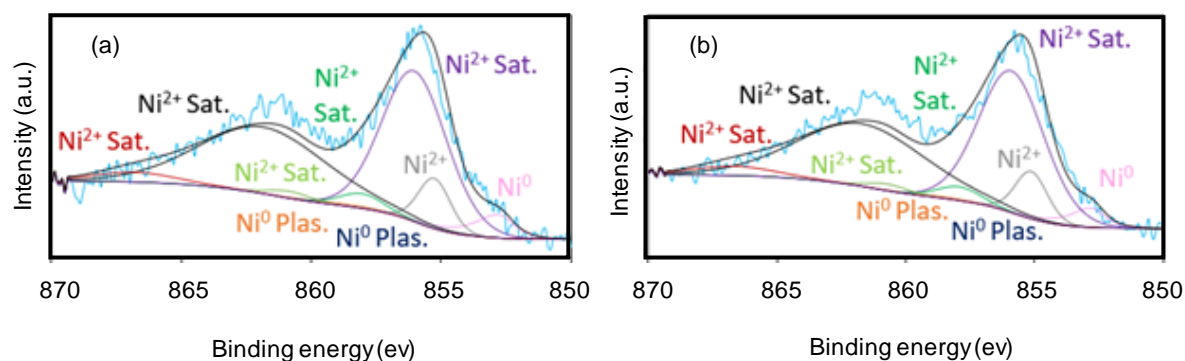

Figure 5. Ni 2p XPS spectra of (a) 4.5%Ru-4.5%Ni/AC, (b) 1%Ru-5%Ni/AC.

15

Table 4. Atomic concentration and surface abundance of Ru and Ni species in carbon-supported catalysts, based on XPS data.

Catalyst	Ru (at%)	Ru oxidation state (%)	Ni (at%)	Ni oxidation state (%)
5.3%Ru/AC	14	Ru^{2+} 100	-	-
4.5%Ru-4.5%Ni/AC	14	Ru^{2+} 100	7	Ni^{2+} 94; Ni^0 6
1%Ru-5%Ni/AC	9	Ru^{2+} 100	10	Ni^{2+} 95; Ni^0 5

These catalysts were also characterized by aberration-corrected scanning transmission electron microscopy (STEM). Results are presented in Figure 6. 5.3%Ru/AC possesses the smallest particles size (1.4 nm) with a good dispersion of Ru particles (Figure 6a-c). Slightly bigger particles are observed in 4.5%Ru-4.5%Ni/AC (2.5 nm, Figure 6d-f) and 1%Ru-5%Ni/AC (2.1 nm, Figure 6g-i), which might be related to the presence of RuNi alloy particles. In any case, such small particle sizes correlate well with the CO chemisorption results (< 4 nm) (Table S2). The slight increase of the particle size between 5.3%Ru/AC, 1%Ru-5%Ni/AC and 4.5%Ru-4.5%Ni/AC respectively could be related to the bimetallic character, or rather to the increase in the Ni loading.[26]

TEM-EDS elemental mapping confirms the homogeneous elemental dispersion of Ru and Ni (Figure 7 for 1%Ru-5%Ni/AC and Figures S6-S8 for the other compositions). Figure 7a shows a representative high angle annular dark-field (HAADF) image of the 1%Ru-5%Ni/AC catalyst. Metal particles smaller than 5 nm were found evenly dispersed on the carbon support. The composition of these particles was elucidated using energy-dispersive X-ray spectroscopy (EDS) presented in Figure 7b. Ru and Ni cover the same areas and a clear separation was not detected. Therefore, the intimate contact and the homogeneous scattering between Ru and Ni indicate that the nanoparticles correspond to RuNi alloys.
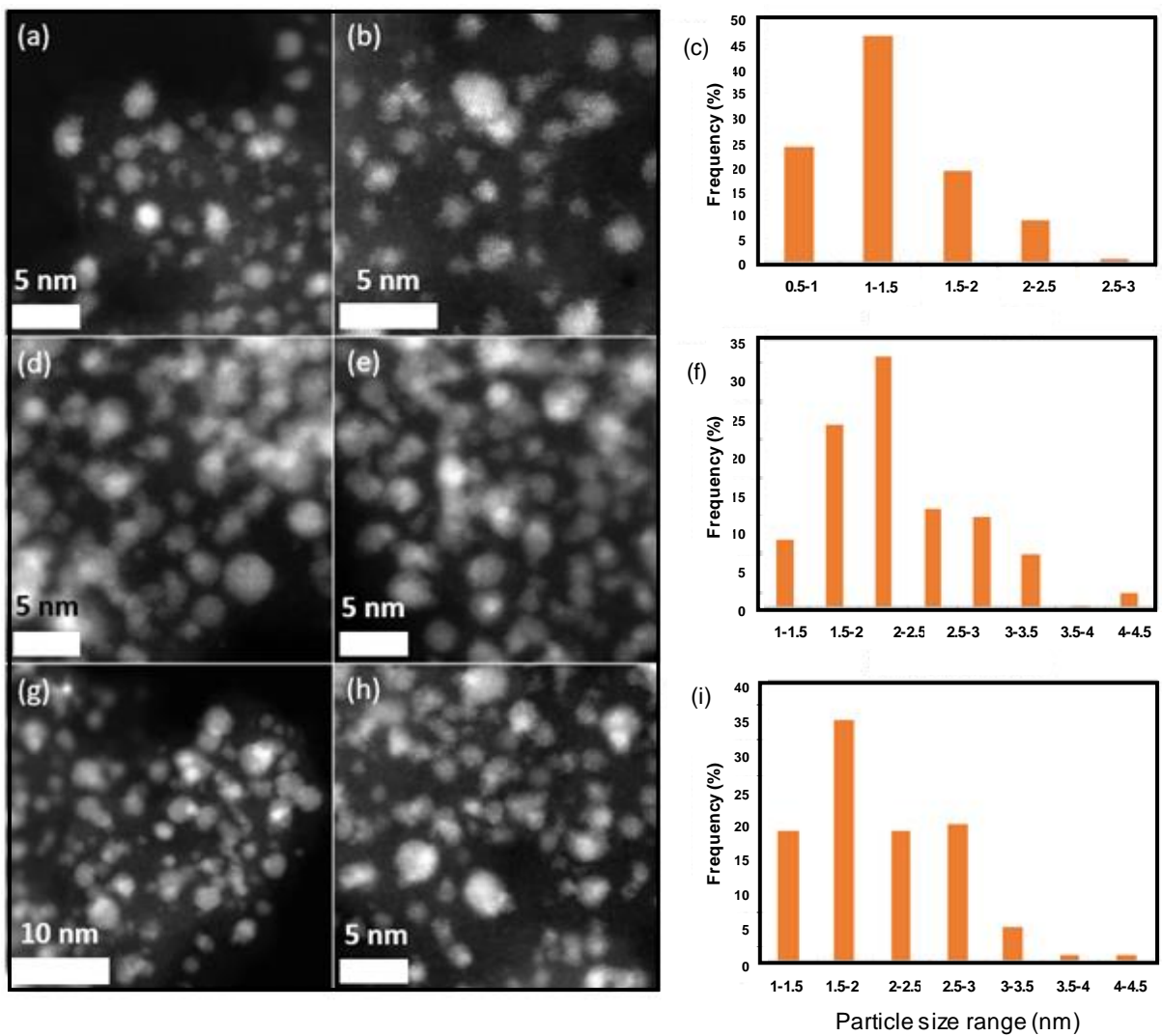
Figure 6. HAADF-STEM images and associated particles (100) size distribution histogram of (a, b, c) 5.3%Ru/AC, (d, e, f) 4.5%Ru-4.5%Ni/AC, (g, h, i) 1%Ru-5%Ni/AC.
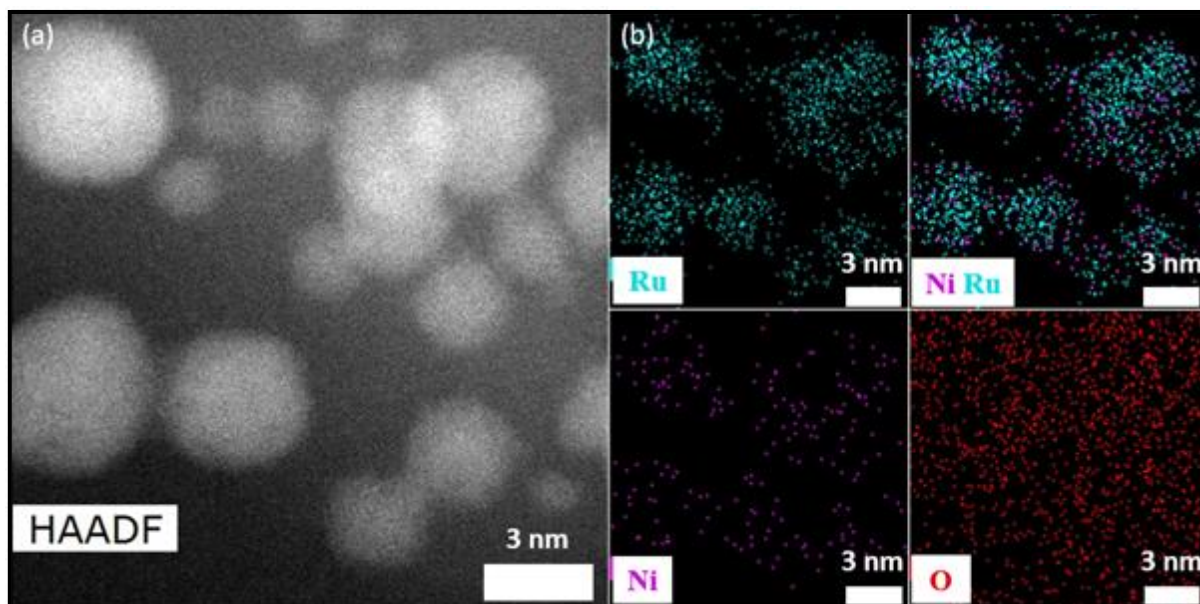
Figure 7. (a) HAADF-STEM; (b) TEM-EDS elemental mapping images of 1%Ru-5%Ni/AC.

3.2.2. Catalytic application

The bimetallic Ru-Ni/AC catalysts were then tested in the amination of hydroxyacetone under the best reaction conditions obtained with 5%Ru/AC (65 °C, 60 bar of H_2, see Section 3.1).

The results obtained after 3 h are presented in Figure 8. Here also, the conversion was of 100%. We noticed that the incorporation of Ni had a significative influence on the catalytic results. For example, the 4.5%Ru-4.5%Ni/AC system gave a yield of 2-aminopropanol up to 53%. Moreover, it was very selective into this amine since the only by-product was propylene glycol. Variations of the Ru and Ni proportions did not lead to significant changes on the selectivity. It is worth noting that the carbon balance in liquid phase was always consistent with the product quantified by NMR analyses. Besides there was still a gap of %C and here the best result was obtained with 4.5%Ru-4.5%Ni/AC (80%, *i.e.* 20% of products are not present in liquid phase). One may note that while the 1%Ru/AC gave poor results (10% of amines), when associated to 5%Ni, the resulting 1%Ru-5%Ni/AC gave a cumulated yield of more than 55% of amines with an additional yield in propylene glycol of 10%.

In summary, bimetallic Ru and Ni systems are very efficient to transform hydroxyacetone into 2-aminopropanol despite the competitive hydrogenation into propylene glycol. There is an evident synergy of the two alloyed metals as deduced from the increase of amines yields following Ni introduction (from 42% for 5.3%Ru/AC to 52% for 4.5%Ru-4.5%Ni/AC) as well as amines selectivity following the reduction of Ru content.

18

These values are slightly lower than that obtained with the singular single-crystal Co_2P nanorods,[13] but much higher than that obtained with a closer system Ru/ZrO_2.[10b]

In the composition range we investigated, it appears difficult at this stage to definitively attribute the actual role of each metal species. However some elements can be drawn from the literature, especially from the recent Perspective paper from Wang and coll. who proposed that the chemical state of the metallic species at the surface (reduction degree) plays a role on the adsorption of the different intermediates (amines, imines, Schiff base), and on the hydrogenation capacities, Ru being crucial for imine reduction,[18] and can play a role on the direct hydrogenation of hydroxyacetone to propylene glycol.[27]

We performed a set experiments to investigate the influence of each metal (detailed results are presented in Table S3 in Supplementary information). First, we studied hydroxyacetone reductive amination with 5.5%Ni/AC and low conversion was observed, with very limited formation of alaninol and no formation of PG even under more demanding conditions. This indicates a lower reductive power for Ni catalysts compared to Ru catalysts. Then, we compared the efficiency of two Ru-Ni/AC compositions for the reduction of hydroxyacetone into propylene glycol (under conditions adapted to avoid full conversion). 4.5%Ru-4.5%Ni/AC gave a much higher conversion than 1%Ru-5%Ni/AC, confirming the higher ability of Ru for hydrogenation in such systems.

This is consistent with the literature. As recently reviewed, Ru catalysts present higher reaction rates than other metals for the aqueous phase hydrogenation of carbonyls functions in biosourced reactants, water associated to Ru playing a predominant role.[28] This point is clearly documented for the reduction of hydroxyacetone for which Ru based catalysts are active under less demanding conditions than for Ni-based catalysts (*eg* 25-50 *vs* 150 °C).[29]

As a conclusion, in our case the 1%Ru-5%Ni composition presents the best compromise in terms of activity and selectivity to the primary amines formation *vs.* side reduction into propylene glycol.
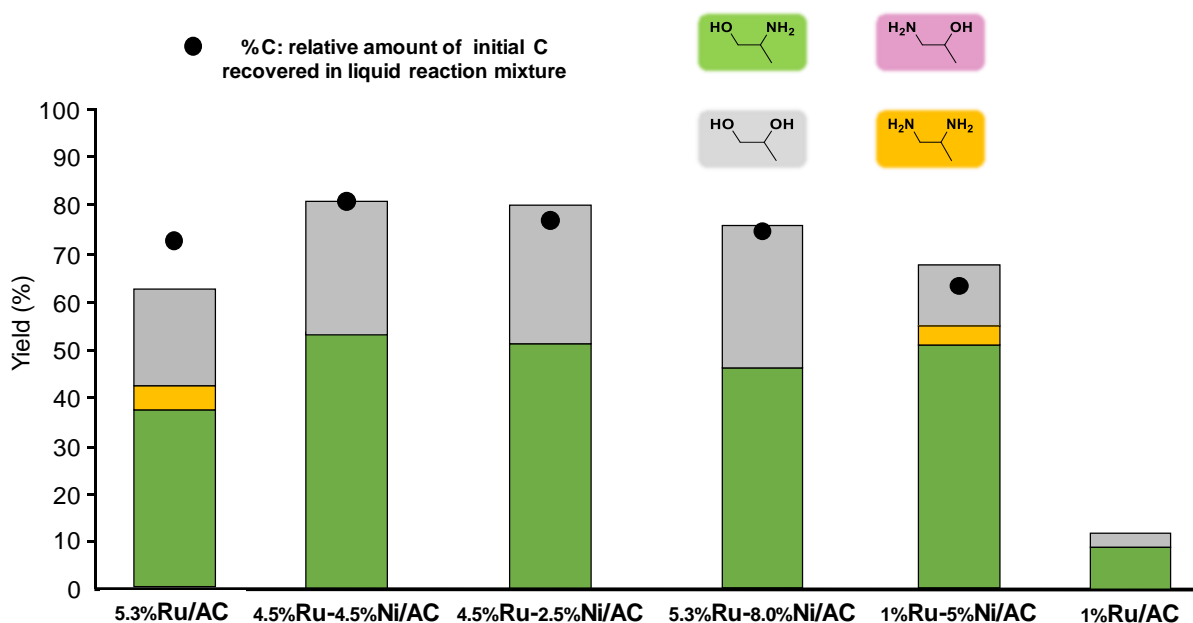
19

Figure 8. Hydroxyacetone amination with Ru-Ni/AC catalysts. Conditions: 100 mL of 25% aqueous NH_3, 10 g of hydroxyacetone, 1 g of catalyst, 65 °C, 60 bar H_2, 3 h. Acetol conversion was 100%.

Note that we investigated the stability of the different products separately under the same reaction conditions (with a different catalytic system). This is presented in Supplementary information (Figures S9 and S10). Globally, 2-aminopropanol and propylene glycol showed to be stable at 95 and 70%, respectively, indicating that some side-reactions occurred on these products, however not towards aminated products.

3.3. Recycling studies with 4.5%Ru-4.5%Ni/AC catalyst

Results presented in Figure 2 seem to indicate that different reaction times imply a variation of products repartition despite a complete conversion. Such variations are expected in the case of deactivation of the catalyst. Recycling studies have been performed with the 4.5%Ru-4.5%Ni catalyst (see Experimental section for details) (Figure 9). First, the catalyst is sufficiently stable to be reused for 3 cycles. Here also only 2-aminopropanol and propylene glycol were obtained with a non-significant variation of repartition (Figure 9a). Some Ru and Ni species are lixiviated as measured by ICP-OES. Especially, the relative loss of Ni in solution was found to increase over the 3 runs but remained limited to a total of 8% of the initial amount of catalyst (Figure 9b). Besides Ru loss was in the range of 15%, which is still relatively limited. A hot filtration experiment was conducted with the 5.3%Ru-8%Ni catalyst in order to assess the

activity of leached ions from the catalyst (Figure 9c). For that the catalyst was removed from the reaction mixture at the reaction temperature after a first run (Run 1'), and a reaction was performed in the absence of catalyst after addition of fresh hydroxyacetone (Run 2'). As a result, the concentration of products after Run 2' was comparable to that quantified after Run 1', therefore the Ru and Ni leached species (8 and 3% from catalyst content, respectively) did not contribute to the formation of the target products. Note that these experiments were performed at 100% of hydroxyacetone conversion. Performing recycling at a much lower conversion was not possible due to the fast reactivity of hydroxyacetone. These studies give nevertheless a good view of the recyclability potential of such catalysts.
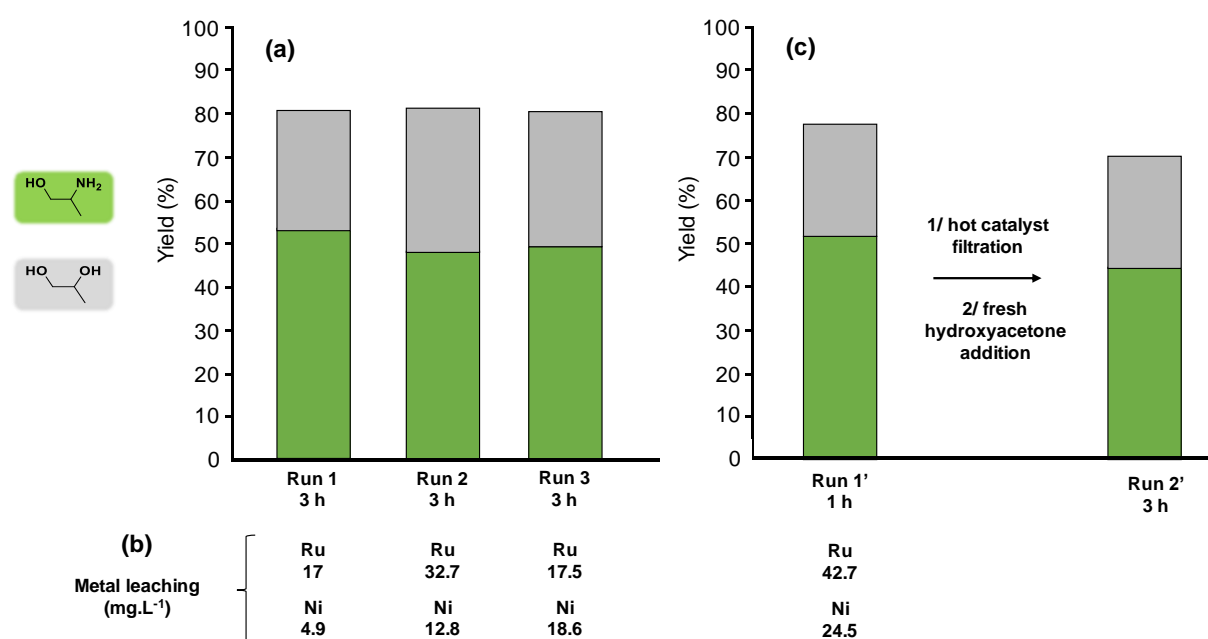

Figure 9. (a) Reusability of 4.5%Ru-4.5%Ni/AC; (b) Leaching extent of metals into the liquid phase after each run with initial metals content of 450 mg.L^{-1} for both Ru and Ni from 4.5%Ru-4.5%Ni/AC. (c) Efficiency of leached species from 5.3%Ru-8%Ni/AC with initial metals content of 530 mg.L^{-1} for Ru and 800 mg.L^{-1} for Ni. Conditions set: 100 mL of 25% aqueous NH$_3$, 10 g of hydroxyacetone, 1 g of catalyst, 65 °C, 60 bar H$_2$. For Runs 2 and 3 the amount of hydroxyacetone was adapted to the amount of catalyst. Acetol conversion was 100%.

To further evaluate the effect of this leaching over the properties of the used 4.5%Ru-4.5%Ni catalyst, the latter was recovered and characterized again (Figure S11-S14, Tables S3 and S4). First, XRD analysis does not indicate any structural changes during the catalytic reaction. Thus, the nanoparticles remained sufficiently small and well dispersed to be active. Besides, we noticed a significant decrease of BET surface area down to 430 m^2.g^{-1}, the microporosity being

the most affected. This could be due to the presence of adsorbed organic species. Also, XPS data show that the relative concentration of Ru atoms at the surface was divided by a factor 2 at the benefit of Ni, which is coherent with the predominant lixiviation of Ru compared to Ni observed by ICP-OES. In fact, one hypothesis can be that the lixiviation of Ru concerns Ru not engaged in the RuNi alloys, and therefore this loss does not affect the catalytic behaviour at least for 3 cycles. This information says that it would be possible to further tune and optimize the necessary metal contents. Although being an essential point of sustainability, this aspect of catalyst development needs much more investigation and falls outside of the scope of this paper.

3.4. Reactivity of hydroxyacetone biosourced precursors

Finally, we attempted to get the aminated products directly from the biosourced precursors of hydroxyacetone, this in order to go further into the direct use of biomass to minimize the environmental impact of such transformations. Here, in addition to reductive amination, the reactivity involves a C-C bond cleavage (retro-aldol) in the precursor carbon chain. As presented in the Introduction, the group of Sels reported the formation of alkyl diamines by reacting glucose or xylose with alkyl amines under H_2 in the presence of a Ru/C catalyst.[3b] However, no example was reported with NH_3.

We assessed the reactivity of Ru-Ni/AC and Ni/AC catalysts and no target amination was observed (data not presented). Therefore, we tested a 5%Ni-30%W_2C/AC catalyst, that is known to be efficiency for the retro-aldol cleavage of (poly)saccharides leading to glycols under H_2, thanks to the presence of W carbide.[2, 30] Here, for the amination of hydroxyacetone with NH_3, a poor yield of less than 10% of aminated products was obtained. Therefore, the presence of Ru is necessary and a Ru-W_xC/AC catalyst was considered as the best option. However, while catalysts like Ru/WC[31] or Ru-W/C[32] are known, the system Ru-W_xC/AC has never been described. Here we successfully prepared this material by co-impregnation of Ru and W precursors followed by a carburation under H_2 flow at 700 °C (see Experimental section for details). We obtained a 7.5%Ru-36%W_xC/AC material despite targeting a loading of 5 wt% of Ru and 30 wt% of W (to be coherent with the 5%Ni-30%W_2C/AC catalyst). The slight difference is due to the difficulty of accurately control the carburization process that may lead to loss of carbon support. Nevertheless, the metal loading is very close and pertinent enough to apply this system in the catalytic transformation. Characterization data are presented in

Supplementary information (Figures S15-S18, Tables S5 and S6). The XRD diffractogram indicates that the W species consist of a mixture of W_2C (main peaks at $2\Theta = 34.5°, 39.3°$ and $37.9°$, ICSD 00-035-0776) and WC (main peaks at $2\Theta = 31.4°, 35.6°$ and $48.3°$, ICSD 00-051-0939) hexagonal carbides. The wide peak at $2\Theta = 43.4°$ corresponds to small nanoparticles of hexagonal metallic ruthenium. 7.5%Ru-36%W_xC/AC exhibits particles with an average size of 30 nm with a good dispersion of Ru particles on the W aggregates, based on TEM analysis. The presence of large particles is consistent with the high metal loading that was impregnated on the surface. Note that differences exist compared to the Ni-W_xC/AC system for which only the W_2C phase was observed along with NiW and NiWC alloys.[2] Also, a noticeable decrease in the surface area is observed for 7.5%Ru-36%W_xC/AC (593 $m^2.g^{-1}$, compared to the commercial AC, 905 $m^2.g^{-1}$), that was less significant with Ni-W_xC/AC. This could be associated to the higher metal loading. Such high loading should induce: (1) a significant carbon porosity restructuration during thermal treatment steps and sintering of the W and Ru phases; (2) the significant increase in weight density of the material with the decrease of the carbon proportion; (3) the reduction and formation of CH_4 from carbon in the presence of Ru. Concerning XPS analysis for 7.5%Ru-36%W_xC/AC, 3 main peaks of C 1s spectrum are identified, located at 290.2 eV, 286.2 eV and 284.5 eV and corresponding to C-C, C-O and C-C bonds, respectively (unlike 5.3%Ru/AC, the peak assigned to C=O does not appear).[21] Two oxidation states of Ru can be observed on Ru 3d spectrum: metallic ruthenium Ru^0 ($3d_{5/2}$: 279.9 eV and $3d_{3/2}$: 284.2 eV), and $Ru(OH)_2$, from the passivation layer ($3d_{5/2}$: 281 eV and 1 satellite : 283.7 eV; $3d_{3/2}$: 285.3 eV and 1 satellite : 287.9 eV ; the same as for 5.3%Ru/AC).[22a] The Ru $3p_{3/2}$ spectrum displays peaks at 458 eV and 467.8 eV (satellite peak) that are assigned to metallic Ru, while those at 462.5 eV and 465.5 eV (satellite peak) are correlated to $Ru(OH)_2$. Two tungsten species are detected: (1) W_xC ($4f_{7/2}$: 31.46 eV and $4f_{5/2}$: 33.64 eV); (2) W^{6+} ($4f_{7/2}$: 35.6 eV, $4f_{5/2}$: 37.78 eV). Tungsten is highly oxidized on the surface (81% of WO_x). The presence of oxycarbides at the surface of tungsten carbide catalysts is well known. These phases exhibit non-stoichiometric properties, since the lattices exhibit a significant number of oxygen vacancies.[33] These oxygen vacancies enhance the surface conductivity of catalysts,[34] and thus the transfer of electrons and charged particles. These properties, in addition to the high reduction/carburization temperature (700 °C) must explain the partial reduction of Ru^{2+} to Ru^0 (7%), which was not observed for the RuNi/AC catalysts (reduced at 450 °C). 7.5%Ru-

36%W$_x$C/AC presents 10 at% of Ru (lesser than in 5.3%Ru/AC) and 45 at% of W concentrations on the surface.

Concerning the catalytic application of 7.5%Ru-36%W$_x$C/AC, before applying this system to the conversion of saccharides, we first tested it to the reductive amination of hydroxyacetone. A global amine yields around 30% was obtained with in details, 25% of 2-aminopropanol, 3% of 1,2-diaminopropane, 1% of 1-aminopropan-2-ol, and 25% of propylene glycol.

Encouraged by this result, we then studied the reactivity of its direct precursor, glucose, with the expectation that the W$_x$C sites would perform the retro-aldol cleavage of glucose into hydroxyacetone, and the Ru sites the reductive amination into target products. However, despite varying the reaction conditions, we did not observe aminated products. Changing the substrate to fructose, a certain reactivity was observed, with a total yield of aminated products of 9% (Figure 10) including 2-aminopropanol (1%) and 1,2-diaminopropane (1%). Interestingly amines derived from ethylene glycol, especially ethanol amine (5%), were also observed. Note that increasing reaction time up to 8 hours and/or lowering temperature did not gave higher yields.
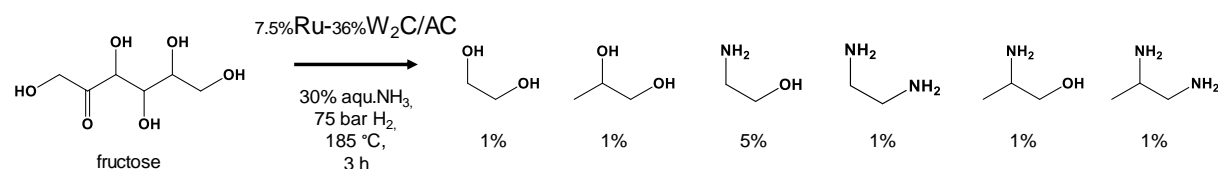

Figure 10. Fructose transformation into amino-derivatives of ethylene and propylene glycol. Conditions: 10 g fructose, 1 g 7.5%Ru-36%W$_x$C/AC, 300 mL of 25% aqueous NH$_3$, 180 °C, 75 bar H$_2$, 3 h.

^{13}C NMR spectra of reaction mixtures obtained after glucose and fructose transformations are presented in Figure S19. In the case of glucose, the presence of many signals in the aromatic area may be due to furan derivatives, which are not present with fructose. It is well known that fructose is more reactive than glucose, for example for dehydration reactions. Apparently, it is also more prone to undergo fast amine attack on the carbonyl site leading to linear aminated products rather than aromatic compounds.

7.5%Ru-36%W$_x$C/AC was not able to aminate neither ethylene nor propylene glycol in these conditions (data not presented). Therefore, the formation of the amines from these sugars

clearly comes from the reductive amination of the carbonylated intermediates, glycoaldehyde and hydroxyacetone. While the reactivity of sugars remains limited, with the one-pot production of primary amines leading to low yields due to the use of ammonia, this study represents the first example of primary amines obtained from the heterogeneously catalytic aminolysis of sugars.

To advance towards an even greener transformation with the challenge to start from cellulose, the two consecutive steps (retro-aldol C-C cleavage and reductive amination) were conducted separately. In the previous work of Zhang *et al*., soluble H_2WO_4 was used to form glycolaldehyde, that was then aminated into ethanol amine.[10b] For our study, the heterogeneous system W_2C/AC was chosen for the first step in place of H_2WO_4 (the synthesis and characterization of this catalyst have been presented elsewhere[2, 35]). Here, we obtained 12% yield of hydroxyacetone from cellulose (Figure 11), which is notably lesser (35-60%) than in recent studies using bi-metallic systems including Ni-SnO$_x$/Al$_2$O$_3$,[36] Sn-Si/C,[37] Sn-Ni/SiO$_2$,[38] or SnFe/C under similar conditions.[39] After this first stage, the 30%W_2C/AC catalyst was removed by filtration, then 50 mL of NH_3 aqueous solution and 0.70 g of 7.5%Ru-36%W$_x$C/AC catalyst were added in the reaction mixture containing hydroxyacetone among all other components (sugars, liquefied cellulosic oligomers…). Here, a certain reactivity was observed and it was possible to obtain 2-aminopropanol and propylene glycol in 18 and 27% yield respectively, relative to hydroxyacetone, and corresponding to 2% yield of 2-aminopropanol relative to cellulose.
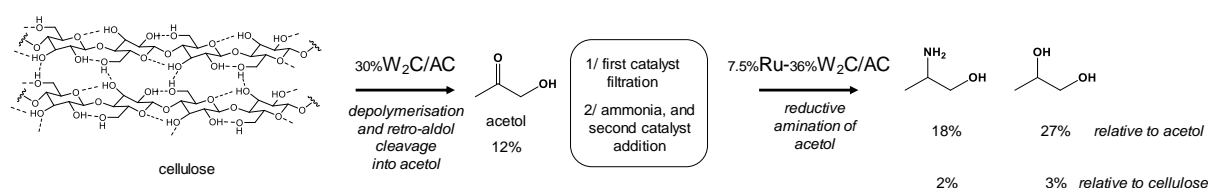

Figure 11. Sequential transformation of cellulose into 2-aminopropanol via hydroxyacetone formation. Conditions: Step 1: 2 g cellulose, 0.75 g 30%W_2C/AC, 100 mL H_2O, 40 bar H_2, 235 °C, 0.5 h; Step 2: 100 mL H_2O + 50 mL of 30% aqueous NH_3, 0.70 g 7.5%Ru-36%W$_x$C/AC, 75 bar H_2, 65 °C, 3 h.

The yields into aminated products obtained from (poly)saccharides in the study described in this section may appear low. However, they correspond to the first example of these transformations, and particularly this is the first time that such aminated product was

obtained from cellulose by a 2-steps procedure furthermore involving heterogeneous catalysts.

4. Conclusion

We reported in this paper an overall study on the reductive amination of bio-sourced substrates by NH_3, from simple reactant to a polycarbohydrate with heterogeneous efficient and robust heterogeneous catalysts. We prepared and fully characterized a family of Ru-Ni/AC catalysts synthesized by a co-impregnation route. Such catalysts have been used for the first time for the reductive amination of hydroxyacetone and a 4.5%Ru-4.5%Ni/AC system showed to be very efficient in the presence of aqueous NH_3 to form primary amines derived from propylene glycol (65 °C, 60 bar H_2, 3-5 h). A certain synergy between Ni and Ru has been demonstrated and up to 55% amines yield was obtained including 50% of 2-aminopropanol. The potential of catalyst reuse was assessed during 3 successive cycles demonstrating a good reusability of the material. We also explored the direct reductive aminolysis of sugars. For that an original catalyst 7.5%Ru-36%W_xC/AC was prepared by one-pot co-impregnation and carburization and characterized. Starting from fructose, this catalyst gave up to 9% of primary amines (aqueous NH_3, 180 °C, 75 bar H_2, 3 h), which is the first example of the formation of primary amines directly from carbohydrates. To go further, we used a combination of 30%W_2C/AC and 7.5%Ru-36%W_xC/AC for a sequential transformation of robust cellulose into aminated derivatives through the intermediate formation of hydroxyacetone (40 bar H_2, 235 °C, 0.5 h), and 2% of 2-aminopropanol were obtained which is the first example of the formation of this primary amine from cellulose and in the presence of only heterogeneous catalysis. By reacting biosourced substrates, in green media and using reusable heterogeneous catalysts, this global study clearly participates to the development of sustainable chemical transformations, in this case for the formation of important aminated products.

from Maya Marinova (TEM), Laurence Burylo (XRD) from Chevreul Institute Pascal Bargiela (XPS), Pascale Mascunan and Nicolas Bonnet (ICP-EOS analysis) from Ircatech.

References

[1] a) V. Froidevaux, C. Negrell, S. Caillol, J.-P. Pascault, B. Boutevin, *Chem. Rev.* **2016**, *116*, 14181-14224; b) H. Wu, H. Li, Z. Fang, *Green Chem.* **2021**, *23*, 6675-6697.

[2] F. Goc, T. Epicier, N. Perret, F. Rataboul, *ChemCatChem* **2023**, *15*, e202201496.

[3] a) M. Pelckmans, T. Mihaylov, W. Faveere, J. Poissonnier, F. Van Waes, K. Moonen, G. B. Marin, J. W. Thybaut, K. Pierloot, B. F. Sels, *ACS Catal.* **2018**, *8*, 4201-4212; b) M. Pelckmans, W. Vermandel, F. Van Waes, K. Moonen, B. F. Sels, *Angew. Chem. Int. Ed.* **2017**, *56*, 14540-14544.

[4] a) M. Ullrich, F. Weinelt, M. Winnacker, in Biobased Polyamides: Academic and industrial aspects for their development and applications, *Advances in Polymer Science book series*, Springer Ed. **2022**; b) M. Winnacker, B. Rieger, *Macromol. Rapid Commun.* **2016**, *37*, 1391-1413.

[5] J. Runeberg, A. Baiker, J. Kijenski, *Appl. Catal.* **1985**, *17*, 309-319.

[6] C.-J. Yue, K. Di, L.-P. Gu, Z.-W. Zhang, L.-L. Ding, *Mol. Catal.* **2019**, *477*.

[7] a) E. Podyacheva, O. I. Afanasyev, D. V. Vasilyev, D. Chusov, *ACS Catal.* **2022**, *12*, 7142-7198; b) S. Bähn, S. Imm, L. Neubert, M. Zhang, H. Neumann, M. Beller, *ChemCatChem* **2011**, *3*, 1853-1864.

[8] a) N. K. Gupta, P. Reif, P. Palenicek, M. Rose, *ACS Catal.* **2022**, *12*, 10400-10440; b) S. Hameury, H. Bensalem, K. De Oliveira Vigier, *Catalysts* **2022**, *12*, 1306; c) Y. Rong, N. Ji, Z. Yu, X. Diao, H. Li, Y. Lei, X. Lu, A. Fukuoka, *Green Chem.* **2021**, *23*, 6761-6788; d) M. Pelckmans, T. Renders, S. Van de Vyver, B. F. Sels, *Green Chem.* **2017**, *19*, 5303-5331; e) M. Pera-Titus, F. Shi, *ChemSusChem* **2014**, *7*, 720-722.

[9] a) C. C. Truong, D. K. Mishra, Y.-W. Suh, *ChemSusChem* **2023**, *16*, e202201846; b) J. Liu, Y. Song, L. Ma, *Chem. Asian J.* **2021**, *16*, 2371-2391; c) C. T. Nandhu, T. Aneeja, G. Anilkumar, *J. Organomet. Chem.* **2022**, *965-966*, 122332; d) M. K. Saini, S. Kumar, H. Li, S. A. Babu, S. Saravanamurugan, *ChemSusChem* **2022**, *15*, e202200107; e) N. U. D. Reshi, V. B. Saptal, M. Beller, J. K. Bera, *ACS Catal.* **2021**, *11*, 13809-13837; f) T. Irrgang, R. Kempe, *Chem. Rev.* **2020**, *120*, 9583-9674; g) J. He, L. Chen, S. Liu, K. Song, S. Yang, A. Riisager, *Green Chem.* **2020**, *22*, 6714-6747; h) K. Murugesan, T. Senthamarai, V. G. Chandrashekhar, K. Natte, P. C. J. Kamer, M. Beller, R. V. Jagadeesh, *Chem. Soc. Rev.* **2020**, *49*, 6273-6328; i) Y. Wei, X. Wu, C. Wang, J. Xiao, *Catal. Today* **2015**, *247*, 104-116.

[10] a) W. Faveere, T. Mihaylov, M. Pelckmans, K. Moonen, F. Gillis-D'Hamers, R. Bosschaerts, K. Pierloot, B. F. Sels, *ACS Catal.* **2020**, *10*, 391-404; b) G. Liang, A. Wang, L. Li, G. Xu, N. Yan, T. Zhang, *Angew. Chem. Int. Ed.* **2017**, *56*, 3050-3054; c) B. Kusema, Z. Yan, S. Streiff, WO2021114166, Rhodia Operations, **2021**.

[11] R. Verma, Y. Jing, H. Liu, V. Aggarwal, H. Kumar Goswami, E. Bala, Z. Ke, P. Kumar Verma, *Eur. J. Org. Chem.* **2022**, *2022*, e202200298.

[12] T. Trégner, J. Trejbal, N. Rushswurmova, M. Zapletal, *Chem. Biochem. Eng. Q.* **2017**, *31*, 455-470.

[13] M. Sheng, S. Fujita, S. Yamaguchi, J. Yamasaki, K. Nakajima, S. Yamazoe, T. Mizugaki, T. Mitsudome, *J. Am. Chem. Soc. Au* **2021**, *1*, 501-507.

[14] C.-K. Shin, S.-H. Kim, K.-H. Chang, H.-C. Lee, G.-J. Kim, *Stud. Surf. Catal.* **2006**, *159*, 313-316.

[15] Q.-W. Yu, Y.-N. Li, Q. Zhang, W.-Q. Wang, S.-N. Mei, F. Hui, J. Shi, F.-W. Zhao, J.-M. Yang, J. Lu, *Chem. Pap.* **2019**, *73*, 2019-2026.

[16] C. Eidamshaus, J.-P. Melder, J. Pastre, H.-J. Pallasch, WO2019105782, BASF SE, **2019**.

[17] T. Takanashi, Y. Nakagawa, K. Tomishige, *Chem. Lett.* **2014**, *43*, 822-824.

[18] S. Jia, Z. Chen, Y. Jing, Y. Wang, *ACS Catal.* **2023**, *13*, 13034-13042.

[19] a) D. Cheng, Z. Wang, Y. Xia, Y. Wang, W. Zhang, W. Zhu, *RSC Adv.* **2016**, *6*, 102373-102380; b) J.-M. Jehng, C.-M. Chen, *Catal. Lett.* **2001**, *77*, 147-154; c) Y. Wei, W. Ni, C. Zhang, K. You, F. Zhao, Z. Chen, Q. Ai, H. A. Luo, *ACS Sustain. Chem. Eng.* **2022**, *10*, 13367-13379.

[20] M. Cardona-Farreny, P. Lecante, J. Esvan, C. Dinoi, I. del Rosal, R. Poteau, K. Philippot, M. R. Axet, *Green Chem.* **2021**, *23*, 8480-8500.

[21] D. J. Martin, K. Qiu, S. A. Shevlin, A. D. Handoko, X. Chen, Z. Guo, J. Tang, *Angew. Chem. Int. Ed.* **2014**, *53*, 9240-9245.

[22] a) Z. Ma, S. Zhao, X. Pei, X. Xiong, B. Hu, *Catal. Sci. Technol.* **2017**, *7*, 191-199; b) D. J. Morgan, *Surf. Interface Anal.* **2015**, *47*, 1072-1079.

[23] B. Feng, C. Chen, H. Yang, X. Zhao, L. Hua, Y. Yu, T. Cao, Y. Shi, Z. Hou, *Adv. Synth. Catal.* **2012**, *354*, 1559-1565.

[24] M. C. Biesinger, B. P. Payne, L. W. M. Lau, A. Gerson, R. S. C. Smart, *Surf. Interface Anal.* **2009**, *41*, 324-332.

[25] D. Li, I. Atake, T. Shishido, Y. Oumi, T. Sano, K. Takehira, *J. Catal.* **2007**, *250*, 299-312.

[26] E. Soszka, M. Jędrzejczyk, I. Kocemba, N. Keller, A. M. Ruppert, *Catalysts* **2020**, *10*, 1026.

[27] Y. Wang, S. Furukawa, S. Song, Q. He, H. Asakura, N. Yan, *Angew. Chem. Int. Ed.* **2020**, *59*, 2289-2293.

[28] C. Michel, P. Gallezot, *ACS Catal.* **2015**, *5*, 4130-4132.

[29] a) J. Tan, J. Cui, X. Cui, T. Deng, X. Li, Y. Zhu, Y. Li, *ACS Catal.* **2015**, *5*, 7379-7384; b) D. Duraczyńska, A. Michalik-Zym, B. D. Napruszewska, R. Dula, R. P. Socha, L. Lityńska-Dobrzyńska, A. Gaweł, K. Bahranowski, E. M. Serwicka, *ChemistrySelect* **2016**, *1*, 2148-2155; c) D. Han, W. Yin, A. Arslan, T. Liu, Y. Zheng, S. Xia, *Catalysts* **2020**, *10*, 402.

[30] N. Ji, T. Zhang, M. Zheng, A. Wang, H. Wang, X. Wang, J. G. Chen, *Angew. Chem. Int. Ed.* **2008**, *47*, 8510-8513.

[31] A. Griboval-Constant, J. M. Giraudon, I. Twagishema, G. Leclercq, M. E. Rivas, J. Alvarez, M. J. Pérez-Zurita, M. R. Goldwasser, *J. Mol. Catal. A* **2006**, *259*, 187-196.

[32] a) M.-Y. Zheng, A.-Q. Wang, N. Ji, J.-F. Pang, X.-D. Wang, T. Zhang, *ChemSusChem* **2010**, *3*, 63-66; b) L. S. Ribeiro, J. J. M. Órfão, M. F. R. Pereira, *Bioresource Technol.* **2018**, *263*, 402-409.

[33] C. Di Valentin, G. Pacchioni, *Acc. Chem. Res.* **2014**, *47*, 3233-3241.

[34] a) Z.-F. Huang, J. Song, L. Pan, X. Zhang, L. Wang, J.-J. Zou, *Adv. Mater.* **2015**, *27*, 5309-5327; b) S. H. Hong, S. H. Ahn, J. Choi, J. Y. Kim, H. Y. Kim, H.-J. Kim, J. H. Jang, H. Kim, S.-K. Kim, *Appl. Surf. Sci.* **2015**, *349*, 629-635.

[35] F. Goc, PhD Thesis, Université Claude-Bernard Lyon 1, **2022**.

[36] T. Deng, H. Liu, *J. Mol. Catal. A* **2014**, *388-389*, 66-73.

[37] H. Wang, C. Zhu, Q. Liu, J. Tan, C. Wang, Z. Liang, L. Ma, *ChemSusChem* **2019**, *12*, 2154-2160.

[38] X. Liu, X. Liu, G. Xu, Y. Zhang, C. Wang, Q. Lu, L. Ma, *Green Chem.* **2019**, *21*, 5647-5656.

[39] S.-C. Li, Y.-l. Deng, H.-Y. Wang, C.-G. Wang, L.-l. Ma, Q.-Y. Liu, *J. Fuel Chem. Technol.* **2022**, *50*, 314-325.